Theoretical studies of sequence effects on the conformational properties of a fragment of the prion protein: implications for scrapie formation

Steven L Kazmirski[1], Darwin OV Alonso[1,2], Fred E Cohen[2,3,4,5], Stanley B Prusiner[5,6] and Valerie Daggett[1]*

[1]Department of Medicinal Chemistry, BG-20, University of Washington, Seattle, WA 98195, USA and Departments of [2]Pharmaceutical Chemistry, [3]Medicine, [4]Cellular and Molecular Pharmacology, [5]Biochemistry and Biophysics and [6]Neurology, University of California at San Francisco, San Francisco, CA 94143, USA

Background: Prion diseases are neurodegenerative disorders that appear to be due to a conformational change, involving the conversion of α-helices in the normal, cellular isoform of the prion protein (PrP^C) to β-structure in the infectious scrapie form (PrP^{Sc}). One form of Gerstmann–Sträussler–Scheinker syndrome (GSS), an inherited prion disease, is caused by mutation of Ala117 of PrP^C to Val. We therefore set out to evaluate the effects of this mutation on the stability of the PrP^C form.

Results: We have performed molecular dynamics simulations of a portion of the PrP^C sequence (residues 109–122, termed H1) that is proposed to figure prominently in the conversion of PrP^C to PrP^{Sc}. In particular, beginning with H1 in the α-helical state, the conformational consequences of sequence changes at position 117 were investigated for six hydrophobic mutations. Of these, only the Val mutation was helix-destabilizing. Portions of this mutant peptide adopted and retained an extended conformation during a 2 ns simulation of the peptide in water.

Conclusions: The conformational transitions and structures observed in the simulation of the mutant peptide with Val at position 117 provide insight into the possible early steps in the conversion of PrP^C to PrP^{Sc}.

Chemistry & Biology May 1995, **2**:305–315

Key words: conformational transitions, hydrophobic clusters, molecular dynamics, peptide dynamics, prion diseases

Introduction

Prions are the infectious pathogens that cause a number of transmissible neurodegenerative diseases in mammals [1]. In humans, four prion diseases have been identified: Kuru [2], Creutzfeldt–Jakob disease (CJD), Gerstmann–Sträussler–Scheinker disease (GSS) and fatal familial insomnia (FFI) [3]. Various forms of these diseases can occur sporadically, in an inherited form, or through infection [4,5]. The essential constituent of prions is the scrapie prion protein (PrP^{Sc}), which is chemically indistinguishable from the normal, cellular protein (PrP^C) but exhibits distinct secondary and tertiary structure [6–12]. Much experimental evidence suggests that PrP^{Sc} assists in the conversion of PrP^C to PrP^{Sc}, thus allowing prions to replicate [1,12–14].

Fourier transform infrared (FTIR) and circular dichroism (CD) spectroscopy studies revealed that the conformational transition of PrP^C to PrP^{Sc} involves the conversion of α-helices to β-sheet structure [11]. Unfortunately, high-resolution structural studies (such as X-ray crystallography and multi-dimensional nuclear magnetic resonance (NMR) spectroscopy) of PrP^C and PrP^{Sc} have been thwarted by aggregation of the protein during purification. As a result, structural data are mainly limited to what can be deduced from FTIR and CD [8,11,15–17].

As there is no experimentally determined three-dimensional structure for PrP^C or PrP^{Sc}, Cohen and co-workers have used algorithms that predict protein structure to generate models of the PrP^C conformation [15,18]. The favored model resulting from this work is a four-helix bundle (Fig. 1), which is supported but not defined by the spectroscopic data [18]. In this model, the first of the predicted helices lies between residues 109–122 (H1) (see Figs 1,2) [15]. The isolated H1 peptide, however, forms β-structure in aqueous solution [15], although it does adopt α-helical structure in hexafluoroisopropyl alcohol (HFIP) [15,19]. Two-dimensional NMR studies of a longer PrP peptide from Syrian hamster (SHa) consisting of residues 90–145, which includes H1, suggest that H1 is α-helical under aqueous conditions [20]. The SHa peptide forms a polymeric aggregate rich in β-structure after a matter of days, however [20].

Gerstmann–Sträussler–Scheinker disease is caused by a mutation near the center of the H1 helix involving substitution of Ala117 with Val (the A117V mutation; see Fig. 1) [21–23]. The position of this substitution provides an

*Corresponding author.

© Current Biology Ltd ISSN 1074-5521

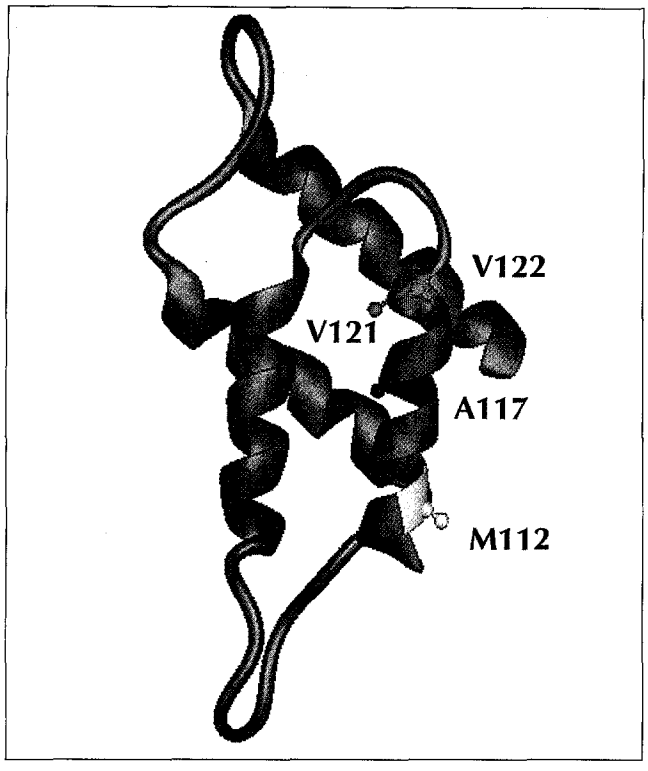

Fig. 1. A predicted three-dimensional model of PrP^C (residues 109–218) [18]. The H1 helix is shown in cyan and specific residues are colored and labeled.

opportunity to test whether the A117V mutation has a destabilizing effect on the helical state, facilitating a conformational change. To this end, we have performed various molecular dynamics simulations of the H1 prion peptide in solution to study the effect of the A117V mutation and other hydrophobic mutations at position 117.

Molecular dynamics has become a common technique for simulating the motion of proteins (reviewed by Daggett and Levitt [24]) and peptides (reviewed by Brooks and Case [25]). To use this method, one must have a well defined starting structure, preferably an X-ray or NMR structure in the case of proteins. This can be a problem for small peptides since they tend to be conformationally heterogeneous and generally one uses models built on idealized conformations to begin a simulation. This technique uses a potential energy function whose parameters have been derived to reproduce structures and energy trends in various model systems. Such a force field can be applied to study a variety of different molecules, including small organic molecules, peptides, lipids, carbohydrates, proteins, RNA and DNA. In molecular dynamics simulations, the atoms move due to their own kinetic energy and the forces exerted upon them by all other atoms. During the simulation one can monitor specific interactions both geometrically and energetically to investigate structural transitions and the mechanism by which they occur. This last point makes the method particularly attractive for investigating sequence effects on the structure of the H1 prion peptide.

Our underlying hypothesis for these simulation studies is that the H1 sequence is helical in PrP^C. Since we are investigating isolated helices, we cannot address the importance of interactions between H1 and the rest of the protein. By making mutations to the helical peptide, however, we can investigate the stability, structure and conformational transitions of the peptide that may be relevant to PrP^{Sc} formation in the intact protein. The term stability refers to the proclivity of the helical structure to unwind (i.e. the rate of unwinding) and not the thermodynamic stability. Simulations of the wild-type sequence and various mutants (A117V, A117I, A117L, A117F and A117NLE; NLE is norleucine, which has an n-butyl group as its side chain and is a common computational and experimental surrogate for methionine) suggest that the A117V mutation destabilizes the helix, while the other mutations do not. These simulations lend support to the contention that inherited prion diseases are a result of a change in the equilibrium between the PrP^C and PrP^{Sc} isoforms of the protein, likely due to an acceleration in the rate of formation of PrP^{Sc} [13,14].

Results

The molecular dynamics of each of the six H1 peptides were simulated for 2.0 ns. Plots of α-helix content versus time are shown in Figure 3 and contour plots of the α-helix content versus time for each residue are shown in Figure 4. Each of these simulations will be discussed below. Table 1 displays a summary of the helix content averaged over the final 0.2 ns for each of the simulations.

Wild-type peptide

Throughout the 2 ns simulation, the wild-type H1 peptide maintained a high percentage of helical structure, seldom falling below 60 % (Fig. 3a). A completely helical structure was never obtained during the simulation as seen by the area of low-percentage helical structure in the plot for residues Gly119 and Ala120 (Fig. 4a). A small, yet strong, hydrophobic cluster near the carboxyl terminus formed between the isopropyl groups of Val121 and Val122 and the methyl group of Ala117. For this interaction to occur, the dihedral angles of Gly119 and Ala120 left the α-helical range to accommodate the strain placed on the backbone. The resulting structure had a partially uncoiled carboxyl terminus and an increase in i→i+5 hydrogen bonds (i refers to the position of a residue in the helix. i+5 is a residue 5 positions towards the carboxyl terminus).

Ace–Met–Lys–His–Met–Ala–Gly–Ala–Ala–Ala–Ala–Gly–Ala–Val–Val–Amd

109 110 111 112 113 114 115 116 117* 118 119 120 121 122

Fig. 2. The sequence of the H1 prion peptide, including acetyl and amide caps. The asterisk indicates the position of the mutation.

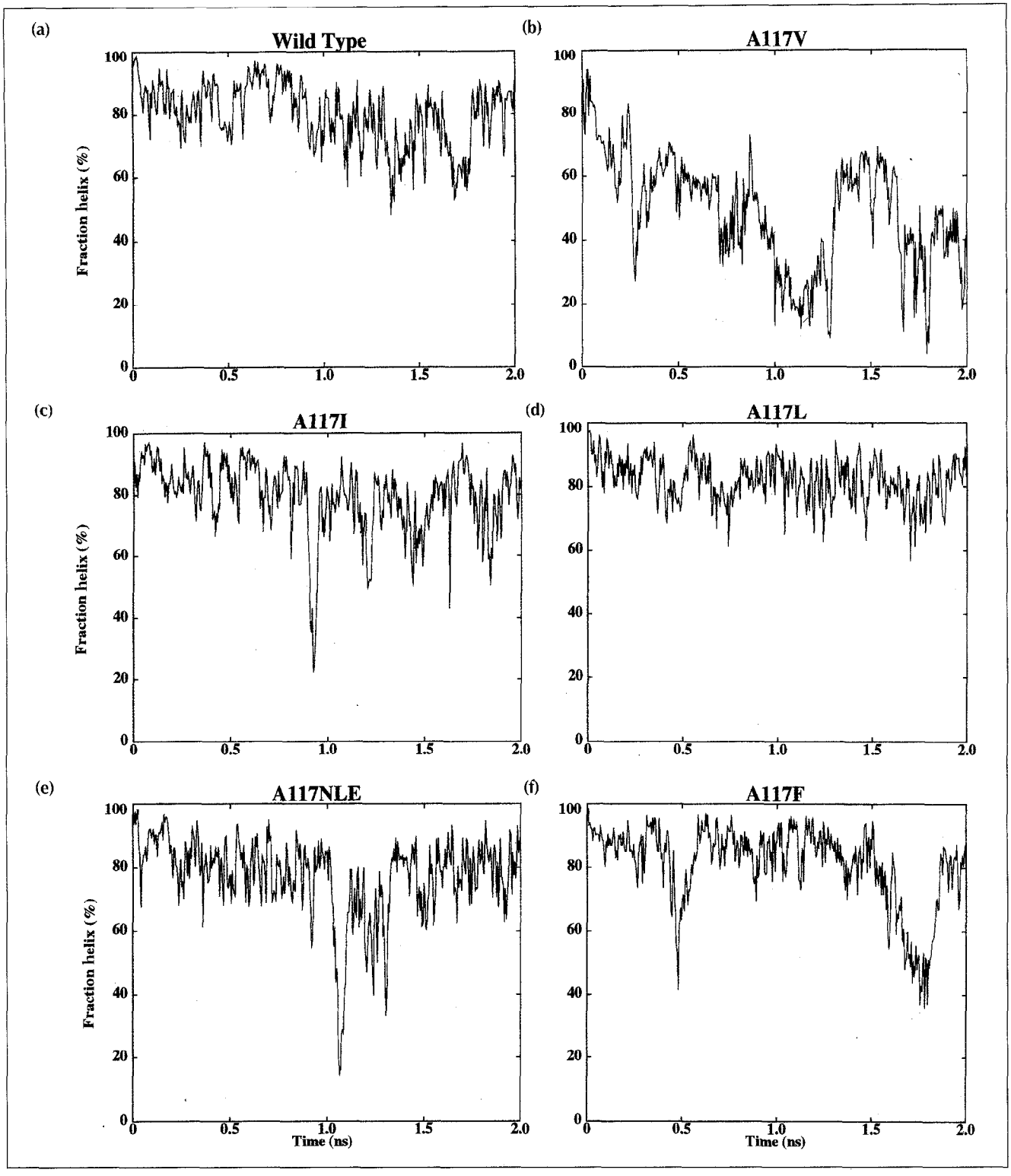

Fig. 3. Percentage α-helical content as a function of time at 298 K for the H1 prion peptides: **(a)** wild type, **(b)** A117V mutant, **(c)** A117I mutant, **(d)** A117L mutant, **(e)** A117NLE mutant and **(f)** A117F mutant.

There were two significant disruptions to the α-helix during the simulation. The first of these occurred slightly before 1.4 ns and involved loss of structure around Lys110 and Met112 (Fig. 4a), such that the side chain of Met112 was incorporated into the carboxy-terminal hydrophobic cluster. The distorted helical structure was short-lived and it was restored through solvation of the side chain of Met112, moving it away from the cluster.

The other significant loss of helix content occurred at ~1.6 ns and involved kinking of the helix due to side-chain clustering between Met112, Val121 and Val122 over the top of the methyl group of Ala117. This arrangement

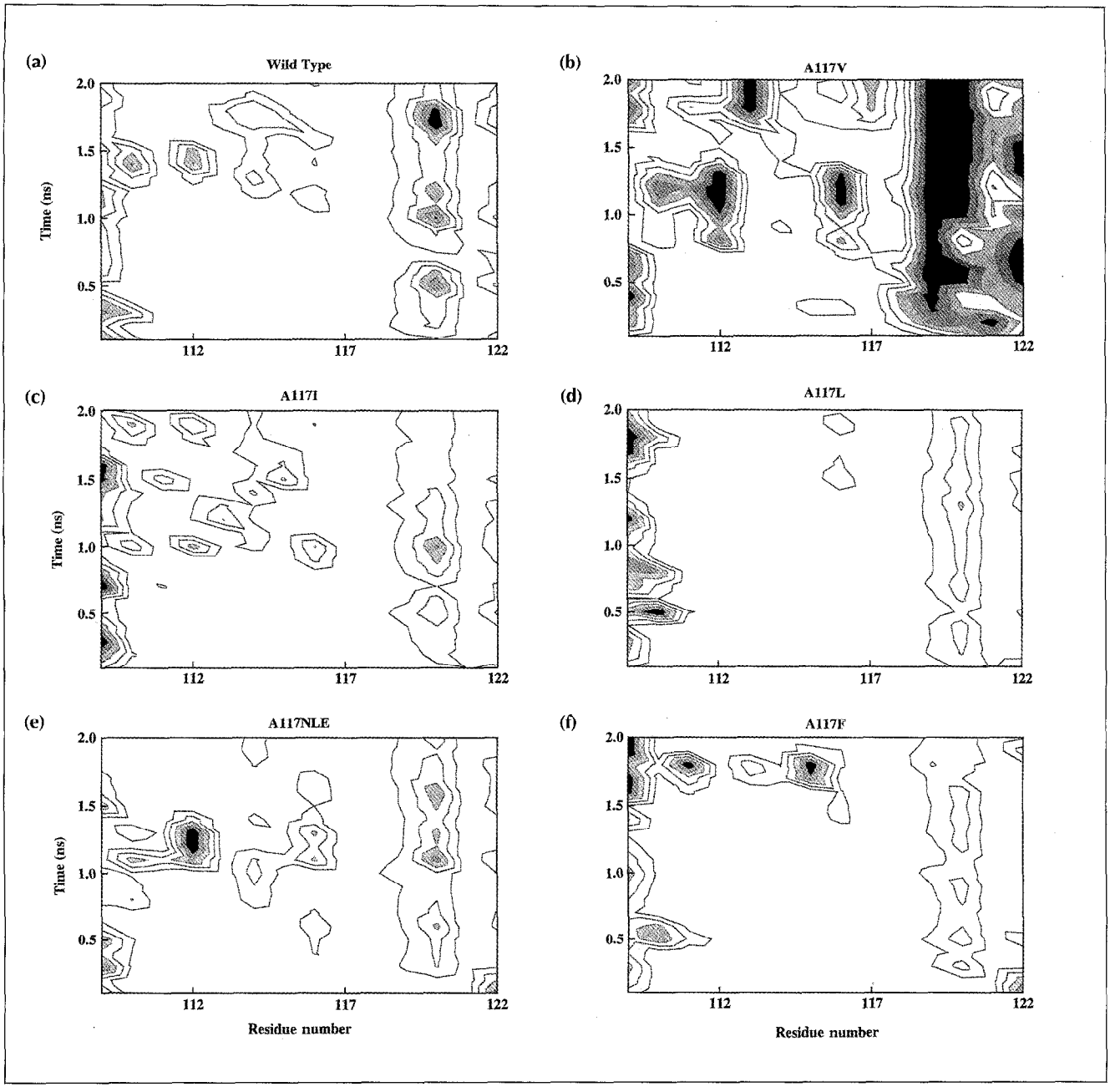

Fig. 4. Contour plots of percentage α-helical structure versus residue number and time for the H1 prion peptides. The contour plots display 'valleys' and 'holes' where α-helix content drops. Shown here are: **(a)** wild type, **(b)** A117V mutant, **(c)** A117I mutant, **(d)** A117L mutant, **(e)** A117NLE mutant and **(f)** A117F mutant. Shades are defined as follows: white (100–83 % α-helix), light gray (83–67 %), medium gray (67–50 %), moderate gray (50–33 %), dark gray (33–17 %), black (17–0 %). If all residues of the peptide were to remain helical, the plot would be white and devoid of contours.

left the main-chain atoms of Ala113, Gly114 and Ala118 accessible to solvent. This conformation was present for ~0.13 ns before Val121 and Val122 moved away and reformed the stable, but smaller hydrophobic cluster described above.

Throughout the simulation, the peptide adopted a structure that appeared to be a 'relaxed helix' near the carboxyl terminus. Unlike an ideal α-helix, which contains i→i+4 and i→i+3 hydrogen bonds, the wild-type H1 peptide contained i→i+4 hydrogen bonds at its amino terminus and many i→i+5 hydrogen bonds at its carboxyl terminus (Fig. 5). These i→i+5 hydrogen bonds helped to stabilize the partial uncoiling of the backbone during the clustering of residues Ala117, Val121 and Val122. However this 'relaxed' helical structure was not unique to the wild-type sequence; all the mutants except for A117V (which adopted a novel structure) formed a significant number of these hydrogen bonds at the carboxyl terminus.

A117V peptide

The α-helix was unstable when Ala117 was mutated to Val (Fig. 3b). Over the first nanosecond of the simulation, the

Table 1. Summary of H1 prion peptide simulations performed and their associated α-helical contents[a].

Peptide	α-Helical content
Wild type	83
A117V	39
A117V[b]	41
A117I	78
A117L	82
A117L[b]	81
A117NLE	81
A117F	75

[a]The α-helical content is the percentage of residues that contained α-helical main-chain dihedral angles averaged over the last 0.2 ns of the simulations. In order for a residue to be considered helical it had to be within a consecutive sequence of three or more residues with α-helical dihedral angles. One residue equals 7 % of the peptide. The standard deviation in the helical content was ~15 %.
[b]Second simulations were performed using slightly different conditions (see Materials and methods).

A117V peptide experienced a steady decline in helix content, owing to the total unwinding of one turn of the α-helix. The second nanosecond of the simulation involved the stabilization of this unwound region of the peptide.

The starting structure for the simulation contained a very tight helix at the carboxyl terminus with many i→i+3 hydrogen bonds (117 NH–114 O, 118 NH–115 O, 119 NH–116 O, 120 NH–117 O and 121 NH–118 O). These hydrogen bonds quickly shifted to i→i+4 hydrogen bonds except for 121 NH–117 O. The β-branched isopropyl groups of Val117 and Val121 prevented the formation of main-chain hydrogen bonding between these residues. As a result of steric clashes between Val117 and Val121, the latter moved above the carboxyl terminus of the helix.

The distortion of Val121 resulted in a large opening for the access of water, and at 0.15 ns, a water molecule inserted itself and became a hydrogen bond acceptor for the amide hydrogens of Val121, Val122 and the amide cap. Gly119 then became more mobile and over the next 0.25 ns made a transition to a left-handed helical conformation, which pointed all residues after Gly119 away from the helix and into solution (Fig. 6).

From 0.9 to 1.3 ns, the peptide formed hydrophobic clusters that stabilized its new, partially unwound conformation. At 0.9 ns, Met112 formed a cluster with Ala116 and Val117 that broke the hydrogen bonds involving Met109, His111, Gly114 and Ala115 and left the main chain accessible to solvent. At 1.0 ns, the side chain of Val121 on the unwound portion of the peptide formed a cluster with the extended methylene chain of Lys110 that persisted for 0.3 ns and further perturbed the helical structure.

At 1.3 ns, Ala120 adopted β-strand dihedral angles (data not shown). This new conformation for Ala120 had two effects on the peptide. First, the amide hydrogen of Ala120 was able to hydrogen bond to the carbonyl oxygen of Gly114, which decreased its rotational mobility. Second, the new dihedral angles of Ala120 rotated the chain of unwound residues and broke up the Val121 and Lys110 cluster. The disruption of this cluster allowed Lys110 to form main-chain hydrogen bonds with Gly114, thus repairing the exposed helix backbone and disrupting the hydrophobic cluster composed of residues 112, 116 and 117. Furthermore, the rotation of the extended residues pointed the carbonyl oxygens of these residues down towards the amino terminus, resulting in a stable interaction with the positive charge on the Lys side chain.

Over the last 0.4 ns of the simulation, Ala113 and Val117 displayed a large decline in helicity (Fig. 4b). Despite this drop, the main-chain hydrogen bond between the two residues increased in strength; the hydrogen bond was intact 29 % of the time between 1.5–1.6 ns and above 90 % of the time for the remainder of the simulation. The adjustment in the backbone of these two residues protected the hydrogen bond from solvent by centering it behind the methyl groups of the alanines 113, 116 and 118 and the side chain of Val117. Furthermore, the distortion of Ala113 moved the side chain of Met112 away from the side chain of Val117, leading to a 33 % increase in the fluctuation of the side-chain dihedral angle χ_1 of Val117.

One must be cautious in basing conclusions on the results of only one simulation. Therefore, another simulation of the A117V peptide was performed using slightly different conditions (see Materials and methods). While details of the trajectory differed, they were very similar overall. The helical structure was again destabilized upon introduction of Val (Table 1). In this simulation, there was an unwinding of the helix beginning at Gly114 leading to a fluctuating turn structure with little resemblance to the initial structure (data not shown).

A117I peptide

In comparison to the A117V simulation, helical structure was well maintained in the A117I simulation (Table 1 and compare Figs 3a,b,c). Throughout most of the simulation, the A117I mutant adopted 'relaxed helix' conformations as described for the wild-type peptide. One interesting thing to note in the plot was the large spike at 0.93 ns where the helical structure dropped close to 0 (Fig. 3c). The loss of structure centered around Met112 because it was incorporated into the small hydrophobic cluster composed of Ile117, Val121 and Val122 (Figs 4,7). This clustering exposed the other side of the helix to solvent (Lys110, His111, Gly114, Ala115 and Gly119).

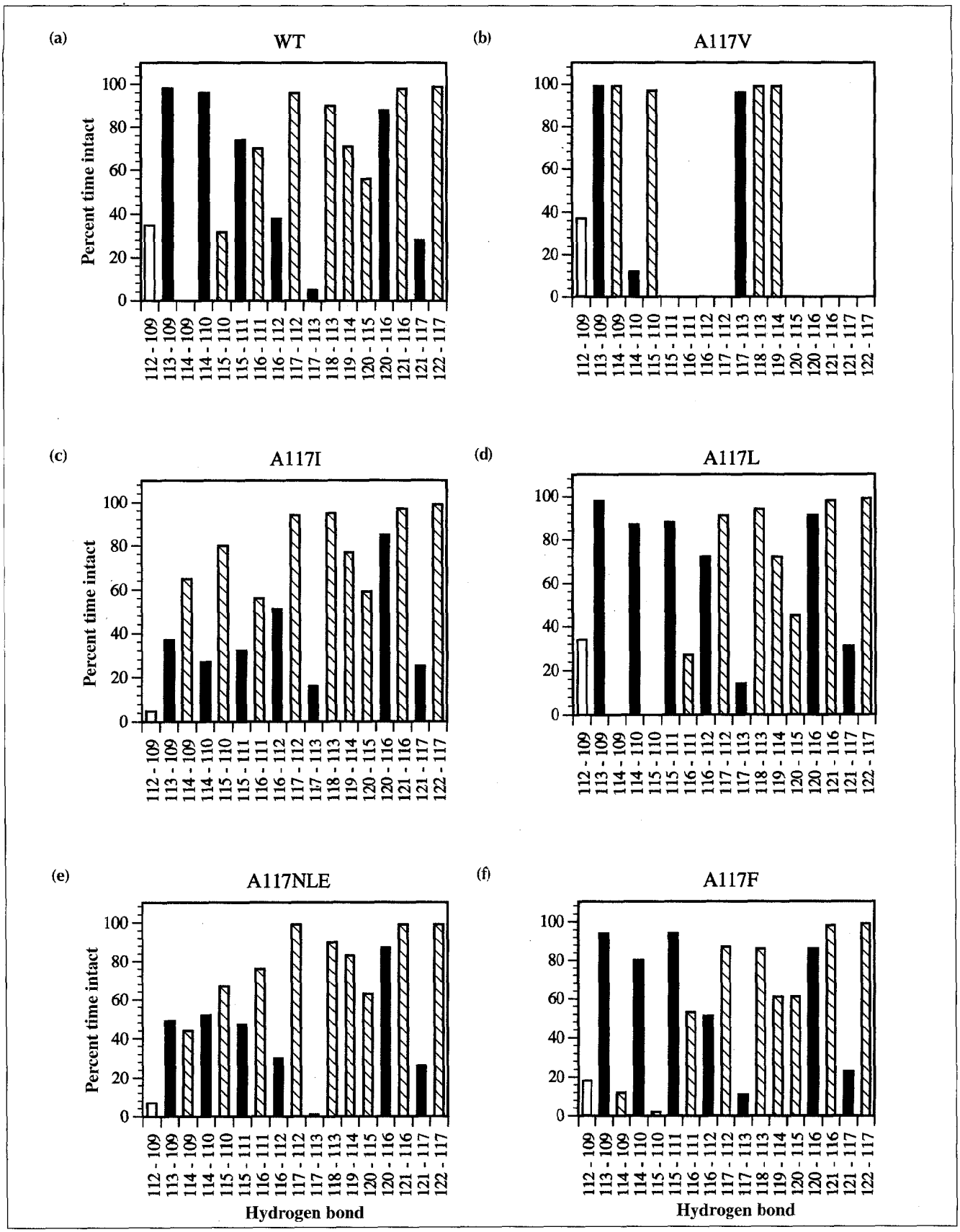

Fig. 5. Hydrogen-bond analysis over the last 0.2 ns of each simulation. **(a)** Wild type, **(b)** A117V mutant, (c) A117I mutant, **(d)** A117L mutant, **(e)** A117NLE mutant and **(f)** A117F mutant. The residues involved are given on the x axis. The solid black bars represent i→i+4 hydrogen bonds. Solid white bars are i→i+3 hydrogen bonds. The slashed bars represent i→i+5 hydrogen bonds. Only hydrogen bonds that were intact ≥ 25 % of the time are shown here. Hydrogen bonds were considered intact when the distance between donor and acceptor atoms was ≤ 2.6 Å.

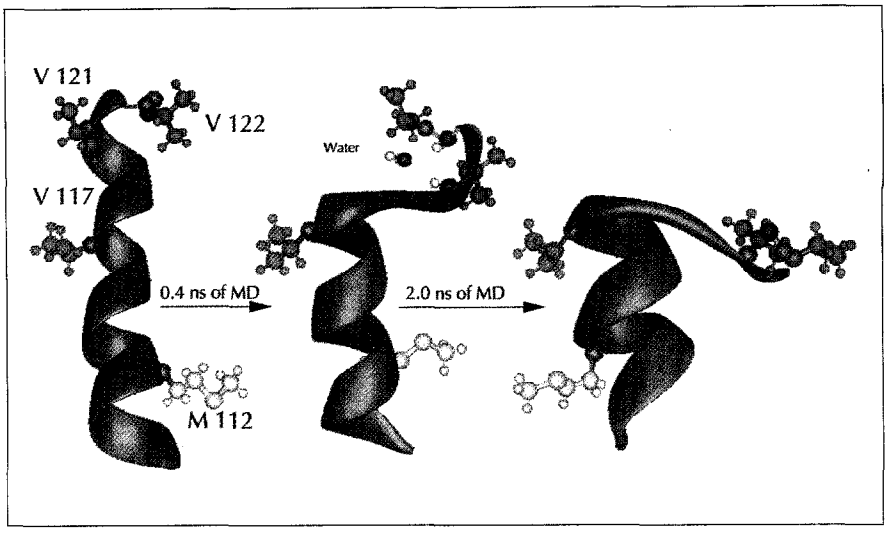

Fig. 6. Snapshots from the A117V simulation illustrating unwinding of the carboxyl terminus of the helix. In the first 0.4 ns, solvation of the last turn of the helix occurred with a 90° rotation of the Val117 side chain. The center and right structures show residues 120–122 pointing out into solution. The adoption of a left-handed helix conformation by Gly119 and β-structure by Ala120 allowed for this conformation. Considering the final structure in the context of the model in Figure 1 suggests that the carboxyl terminus of H1 would point into solution and open the hydrophobic core to solvent.

This arrangement, however, was not stable; the helical content recovered rapidly with the removal of Met112 from the cluster.

Slightly before 1.2 ns, the helical conformation of the A117I mutant experienced another large disruption. Here the dihedral angles of Ala113 became distorted, completely exposing the side chain of Ile117. This distortion of the α-helix allowed the β-branched side chain of Ile117 more freedom to rotate. A 14 % increase was observed in the motion of the χ_1 angle of Ile117. As seen in Figure 3c, this conformation was present for only ~50 ps. After this point, the backbone dihedral angles of Ala113 returned to those of an α-helix.

A117L peptide

The A117L peptide maintained a high degree of helical structure throughout the simulation, ranging between 70–85 % (Table 1, Fig. 3d). Unlike the A117I mutation, the A117L simulation did not experience any large disruptions in helical structure, but instead it suffered three very small distortions. There was a ~15 % reduction in helical content at each of these time points, which corresponds to two residues leaving the helical geometry.

The loss of helical content for the A117L simulation was centered around the amino terminus and Met109 (Fig. 4d). The distortions experienced were associated with Met109 forming contacts with the extended methylene chain of Lys110 and Leu117. This was accomplished by distortion of the main chain around residues 109 and 110 such that the amino terminus moved upwards towards Leu117. A second simulation of A117L, performed under slightly different conditions (see Materials and methods), also showed a high degree of helical structure (Table 1) and was consistent with the description of the fine structure presented above.

A117NLE peptide

The first 1.0 ns and the last 0.6 ns of the A117NLE simulation were very similar to the wild-type simulation (Table 1, Fig. 3). From 1.0 to 1.3 ns, however, the peptide displayed dramatically different behavior. The helical structure of A117NLE changed precipitously at ~1.1 ns. Prior to this, the helix was slightly distorted, as in the wild-type simulation, with a small hydrophobic cluster consisting of Nle117, Val121 and Val122. This small cluster perpetuated the loss of structure in Gly119 and Ala120 (Fig. 4e). Concomitant with the large loss of structure at 1.1 ns, an extensive hydrophobic cluster formed which encompassed the side chains of Met112, Nle117, Val121 and Val122 (Fig. 7). As a result of forming this cluster, one side of the helix collapsed and the other opened up, allowing solvation of the main-chain atoms of residues Lys110, His111, Gly114, Ala115, Ala118 and Gly119.

After ~1.1 ns there was a recovery of some of the helical structure. Previously, Gly114 did not participate in hydrogen bonds and was highly mobile (Fig. 4e), however at ~1.1 ns the amide hydrogens of Gly114 and Ala115 formed hydrogen bonds to the carbonyl group of Met109, decreasing the mobility of Gly114. With the stabilization of Gly114, the backbone of the helix was intact and the helical content increased (Fig. 3e). This conformation was still fairly mobile, however, as seen by the high fluctuation in the helical content over the next 0.2 ns.

A117F peptide

One major difference between Phe and the other hydrophobic residues substituted is the introduction of an aromatic ring that can act as another hydrogen-bond acceptor [26,27]. This property had only a minor effect on the peptide structure, however, as briefly seen at 0.5 ns of the simulation. At this point, a water bridge formed between the ε-amino group of Lys110 and the aromatic ring of Phe117, distorting the helix slightly. This structure was only observed once during the simulation, as the carboxy-terminal half of the helix eventually 'relaxed' to i→i+5 hydrogen bonds that positioned Lys110 on the opposite side of the helix from the Phe ring.

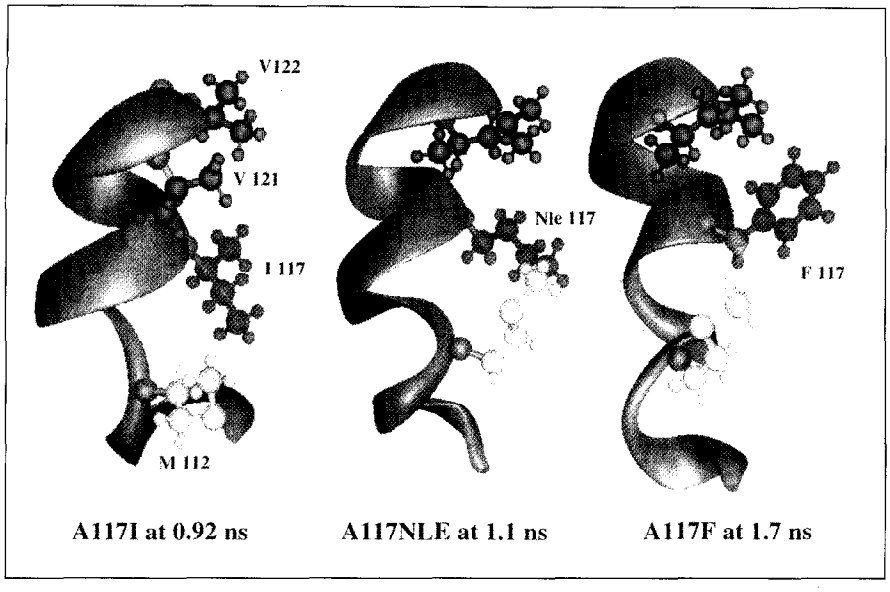

Fig. 7. Three examples of the hydrophobic clusters observed in the simulations. The coloring scheme is the same as that in Figure 6 to facilitate comparison. The clusters distort the helix and leave one face of the helix open to solvent. Each of these peptides has within its cluster the residues Met112, 117, Val121, and Val122. The instantaneous helix content from all three structures is below 40 % and reflects the lowest helix content during the simulations.

Late in the simulation, the A117F mutant lost more than half of its helical structure. This loss correlated with the formation of another hydrophobic cluster similar to the one seen in the A117I and A117NLE simulations. Shortly after 1.6 ns, the Met112 side chain shifted to interact directly with the ring of Phe117 (Fig. 7). The backbone of the helix was strained and the face of the helix opposite this cluster was extensively solvated. The main-chain hydrogen bonds of Met109, Lys110, Ala113, Gly114 and Ala118 were broken, creating a distorted helix reminiscent of the structure observed in the A117NLE simulation; the C_α root-mean square deviation between A117F (1.75 ns) and A117NLE (1.06 ns) was 1.2 Å (Fig. 7). For comparison, the root-mean square deviations between other structures were ≥ 1.6 Å. An explanation for the low root-mean square deviation is that both peptides were distorted through a similar mechanism. In both cases, an extremely large hydrophobic group was placed in the middle of the helix and provided a nucleus for further clustering. Both simulations formed clusters involving residues Met112, 117, Val121 and Val122, which distorted the helix and left one face open to attack by water.

Discussion

Although the biological function of PrP^C has yet to be determined, conversion to PrP^{Sc} is known to be a post-translational process [9,28,29]. Many investigators have resisted the idea that a protein alone could cause a transmissible disease. Despite many years of investigation, no one has been able to identify co-factors or chemical modifications responsible for the conversion of PrP^C to PrP^{Sc} [1,10]. Although the existence of unidentified factors cannot be ruled out, it seems reasonable to assume that a conformational change in PrP^C produces PrP^{Sc}.

Thus, our working hypothesis is that the only difference between PrP^C and PrP^{Sc} is the conformation of the protein [6–8,10–12,17]. Environmental changes, the presence of biological co-factors, or mutations could then shift the equilibrium between the two forms of PrP and favor the development of prion diseases by destabilization of PrP^C, stabilization of PrP^{Sc}, and/or by acceleration of PrP^{Sc} production. Unfortunately, high-resolution structural information for PrP^C and PrP^{Sc} is not available. FTIR and CD spectroscopies have provided some insight into prion protein structure, but the resolution of these methods is limited [8,11,15–17].

Modeling studies represent a logical avenue for attempting to characterize the structural and conformational properties of this system [15,18]. In this modeling study, we have focused on the H1 peptide (Fig. 1), as experimental studies of this fragment suggest that it has a central role in prion diseases [15,18,19,30]. We assume that the H1 section of PrP^C is α-helical for the following reasons: (1) PrP^C contains 42 % α-helical structure and only 3 % β-sheet structure [11]; (2) an extended H1 peptide (residues 104–122) is α-helical in the solid state and in aqueous HFIP [30]; (3) the H1 peptide is α-helical in aqueous HFIP [15,19] and in aqueous SDS [20]; and (4) two-dimensional NMR studies of the SHa peptide (residues 90–145) identify helical structure in the H1 region [20].

To better understand this system and the conformational sensitivity to changes in the sequence, we have performed molecular dynamics simulations of the H1 prion peptide with various amino-acid substitutions at residue 117. Our simulations provide a model of how this portion of the protein might respond to mutations. Although the peptides did not remain ideally α-helical throughout the 2.0 ns simulations, the wild type, A117I, A117L, A117NLE and A117F peptides retained high helix content. In contrast, substitution of Ala117 by Val, a known disease-causing mutation [21–23], led to destabilization of the helix and formation of an extended strand. By destabilization, we are speaking strictly of a kinetic effect and not a thermodynamic effect. To comment on the thermodynamics of the

system, we would require many more trajectories or a much longer simulation time to sample conformational space more effectively. We have completed preliminary studies of seven other mutations at position 117 (A117P, A117D, A117S, A117T, A117W, A117E and A117G). In these cases, two mutations show a significant loss of detailed helical fine structure without a loss of average helical morphology (A117P, A117D), and another develops an extended structure in the carboxy-terminal region of the peptide (A117S) (data not shown). As yet, not one of these mutant peptides exhibits the combination of structural distortions seen in the A117V simulations. Therefore, our results suggest that the conversion of α-helix to an extended structure in the H1 peptide could be involved in the conversion of PrP^C to PrP^{Sc}, and that the A117V mutation facilitates such a conversion.

In general, our simulations are a measure of the destabilization of the H1 helix and do not account for the effect of mutations on other conformations available to the peptide. Upon comparing our helix-destabilizing results with experiments on model helices, it was surprising that we found the Ile and Phe mutants in a helical conformation. In experimental studies, Val, Ile and Phe are helix destabilizing, while Ala, Leu and NLE can easily be incorporated into a helix [31,32]. For the A117V mutant, the loss of helical structure was due to its inability to form a hydrophobic cluster at its carboxyl terminus. The β-branched Val residue at position 117 introduced steric and entropic barriers to forming the cluster. In contrast, the increased hydrophobicity of Ile and Phe made it possible to overcome these entropic barriers and prevent unwinding.

The disruption of the α-helix upon replacement of Ala by Val suggests that the increase in size and hydrophobicity of Val may elicit unfolding. However, comparison of the various simulations indicates that these factors are not enough to destabilize the α-helical conformation of this peptide. For example, all of the mutant residues are more hydrophobic and larger than both Ala and Val, yet they were comparable to the wild-type peptide in terms of α-helical content. Instead, the branched β-carbon of Val created steric conflicts when the backbone was in an α-helical geometry and favored a more open conformation. In contrast, the other β-branched mutant, A117I, was able to form a hydrophobic cluster on one face of the α-helix that exploited the additional hydrophobicity of Ile over Val.

In the predicted model of PrP^C (Fig. 1), the side chain of 117 is pointed directly into the center of the four-helix bundle and contributes to the hydrophobic core [18]. Within the context of this structural model, our results suggest that not only would substitution of Ala by the larger Val presumably be unfavorable due to crowding of the core but it would also facilitate unraveling of the carboxy-terminal end of the helix. This localized unfolding would result in the formation of an extended strand pointing into solution, exposing a portion of the hydrophobic core to solvent or causing a substantial rearrangement of the PrP^C structure. A scenario for the early steps in intermolecular aggregation might be that the extended strand in A117V can interact with another PrP^C molecule to stabilize an alternate conformation on the pathway to PrP^{Sc}. Such a scheme could yield spontaneous formation of disease-causing PrP^{Sc} in patients carrying the A117V mutation of GSS. However, our simulations do not take into account the longer-range interactions possible between the mutant residue and the hydrophobic core of PrP^C, which must also be important in this process.

Significance

Prion diseases are rare neurodegenerative diseases that are believed to be caused by a conformational transition of the normal prion protein (PrP^C) to an abnormal, infectious form (PrP^{Sc}) [1,6–12]. Current difficulties with protein purification and aggregation have prevented structural determination of the prion protein by X-ray crystallography or multi-dimensional NMR techniques. Consequently, theoretical methods have been employed to model the prion protein and its behavior [15,18]. Both theoretical and experimental studies suggest that residues 109–122 (H1) of the prion protein are α-helical in PrP^C and convert to β-structure in PrP^{Sc}. Mutation of Ala117 to Val within this putative helix leads to Gerstmann–Sträussler–Scheinker syndrome, a human prion disease [21–23].

The simulations presented here suggest that mutation of Ala to Val at position 117 destabilizes the H1 helix of PrP^C. Due to steric conflicts in the helical state, Val117 causes the carboxyl terminus of the peptide to unfold and form an extended strand. Simulations of mutants substituted at this position with other hydrophobic residues (A117I, A117L, A117NLE and A117F) suggest that the A117V mutation is unique in its effects upon the H1 helix. Comparison of the helix simulations with the predicted three-dimensional model of PrP^C suggests that disturbance of the H1 helix by the mechanism identified with the A117V peptide may be an early step in the conversion of PrP^C to PrP^{Sc}. This mechanism would expose the hydrophobic core to solvent and the extended strand of H1 would be in a position to interact with neighboring prion proteins, which might facilitate the conversion of other PrP^C molecules.

Materials and methods

The human H1 prion peptide (residues 109–122) in an α-helical conformation was the initial starting point for the simulations (see Figs 1,2). All calculations were performed

using the program ENCAD [33] and a previously described force field [34–36]. The amino terminus was acetylated and the carboxyl terminus was amidated, since experimental studies of this peptide had previously been done [15]. The helices were then subjected to 500 steps of steepest descent minimization *in vacuo* so as to relieve any minor conformational conflicts.

Each minimized structure was then placed into a rectangular box and water molecules were then added at a density of 0.997 g cm^{-3} extending at least 8 Å from any peptide atom. This resulted in the addition of approximately 1000 water molecules (the number differs slightly in the different simulations). Periodic boundary conditions and an 8 Å nonbonded cutoff (with updates to the list every 5 steps) were employed throughout. The water molecules were then subjected to 1000 steps of conjugate gradient minimization. Molecular dynamics (1000 steps at 298 K) was then performed on the water molecules, followed by another 1000 steps of conjugate-gradient minimization to further solvate the peptide. Subsequent to this, the peptide was minimized with 1000 steps of conjugate gradient minimization. Finally, the entire system was minimized for 1000 steps of conjugate gradient minimization.

A molecular dynamics simulation was performed for 2.0 ns at 298 K for each peptide. Each simulation consisted of 10^6 steps of dynamics using a 2 fs time step for evaluating the potential function. Coordinates were saved every 100 time steps, or 0.2 ps, for analysis. Each simulation required ~270 h of computer time on a Silicon Graphics Indy workstation with an R4400 CPU.

For analysis, the percentage of secondary structure was followed throughout the simulation. The backbone dihedral angles were monitored and were evaluated as being either α-helical, β-sheet, or other using a previously described method [37,38]. For a residue to be considered α-helical the following range of backbone dihedral angles had to be satisfied: $-100° < \phi < -30°$ and $-80° < \psi < -5°$. For β-strand conformations, the range was $-170° < \phi < -50°$ and $80° < \psi < 190°$. The helix content plotted in Figure 3 also reflects the repeating nature of helical structure and requires that at least three consecutive residues fulfill the (ϕ,ψ) criterion outlined above. Hydrogen-bond analysis was done using a distance cutoff of 2.6 Å between the relevant donor and acceptor atoms.

To ensure that the basic features observed during the simulation were reproducible, two particular peptides (A117V, and A117L) were simulated a second time under slightly different conditions. A117V and A117L were chosen because they are chemically similar and yet they show very different behavior in the simulations. In these cases, the initial *in vacuo* minimization was omitted. This procedure yields a slightly different starting structure, which results in a different trajectory, and is similar to changing the random number seed or the heating protocol.

Acknowledgements: All molecular graphics images were produced using the MidasPlus program [39] from the Computer Graphics Laboratory, University of California, San Francisco (supported by NIH RR-01081). This work was supported by a program project grant from the National Institutes of Health (AG-02132) to S.B.P. and F.E.C. and start-up funds from the Department of Medicinal Chemistry, University of Washington to V.D.

References

1. Prusiner, S.B. (1991). Molecular biology of prion diseases. *Science* **252**, 1515–1522.
2. Gajdusek, D.C. (1977). Unconventional viruses and the origin and disappearance of kuru. *Science* **197**, 943–960.
3. Collinge, J. & Palmer, M.S. (1992). Molecular genetics of inherited, sporadic and iatrogenic prion disease. In *Prion Diseases of Humans and Animals.* (Prusiner, S.B., Collinge, J., Powell, J., & Anderton, B., eds), pp. 243–255, Ellis Horwood, London.
4. Prusiner, S.B. & Hsiao, K.K. (1994). Human prion diseases. *Ann. Neurol.* **35**, 385–395.
5. Prusiner, S.B. (1994). Inherited prion diseases. *Proc. Natl. Acad. Sci. USA* **91**, 4611–4614.
6. Basler, K., *et al.*, & Weissman, C. (1986). Scrapie and cellular PrP isoforms are encoded by the same chromosomal gene. *Cell* **46**, 417–428.
7. Stahl, N., & Prusiner, S.B. (1991). Prions and prion proteins. *FASEB J.* **5**, 2799–2807.
8. Caughey, B.W., *et al.*, & Caughey, W.S. (1991). Secondary structure analysis of the scrapie associated protein PrP 27–30 in water by infrared spectroscopy. *Biochemistry* **30**, 7672–7680.
9. Caughey, B. & Raymond, G.J. (1991). The scrapie-associated form of PrP is made from a cell surface precursor that is both protease- and phospholipase-sensitive. *J. Biol. Chem.* **266**, 18217–18223.
10. Stahl, N., *et al.*, & Prusiner, S.B. (1993). Structural studies of the scrapie prion protein using mass spectrometry and amino acid sequencing. *Biochemistry* **32**, 1991–2002.
11. Pan, K.-M., *et al.*, & Prusiner, S.B. (1993). Conversion of α-helices into β-sheets features in the formation of the scrapie prion proteins. *Proc. Natl. Acad. Sci. USA* **90**, 10962–10966.
12. Kocisko, D.A., *et al.*, & Caughey, B. (1994). Cell-free formation of protease-resistant prion protein. *Nature* **370**, 471–474.
13. Come J.H. & Lansbury, P.T. (1994). Predisposition of prion protein homozygotes to Creutzfeldt–Jakob disease can be explained by a nucleation-dependent polymerization mechanism. *J. Am. Chem. Soc.* **116**, 4109–4110.
14. Cohen, F.E., Pan, K.-M., Huang, Z., Baldwin, M., Fletterick, R.J., & Prusiner, S.B. (1994). Structural clues to prion replication. *Science* **264**, 530–531.
15. Gasset, M., *et al.*, & Prusiner, S.B. (1992). Predicted α-helical regions of the prion protein when synthesized as peptides form amyloid. *Proc. Natl. Acad. Sci. USA* **89**, 10940–10944.
16. Safar, J., Roller, P.P., Gajdusek, D.C. & Gibbs, C.J. (1993). Thermal stability and conformational transitions of scrapie amyloid (prion) protein correlate with infectivity. *Protein Sci.* **2**, 2206–2216
17. Safar, J., Roller, P.P., Gajdusek, D.C. & Gibbs, C.J. (1993). Conformational transitions, dissociation, and unfolding of scrapie amyloid (prion) protein. *J. Biol. Chem.* **268**, 20276–20284.
18. Huang, Z., *et al.*, & Cohen, F.E. (1994). Proposed three-dimensional structure for the cellular prion protein. *Proc. Natl. Acad. Sci. USA* **91**, 7139–7143.
19. Nguyen, J., *et al.*, & Prusiner, S.B. (1995). Conformation and ultrastructure of prion peptides. *Biochemistry,* in press.
20. Zhang, H., *et al.*, & Prusiner, S.B. (1995). Conformational transitions in peptides containing two putative α-helices of the prion protein. *J. Mol. Biol.,* in press.
21. Doh-ura, K., Tateishi, J. Sasaki, H., Kitamoto, T. & Sakaki, Y. (1989). Pro→Leu change at position 102 of prion protein is the most common but not sole mutation related to Gerstmann–Sträussler syndrome. *Biochem. Biophys. Res. Commun.* **163**, 974–979.
22. Hsiao, K.K., *et al.*, & Prusiner, S.B. (1991). A prion protein variant in a family with the telencephalic form of Gerstmann–Sträussler–Scheinker syndrome. *Neurology* **41**, 681–684.
23. Mastrianni, J.A., *et al.*, & Garbern, J.Y. (1995). Prion disease (PrP-A117V) presenting with ataxia instead of dementia. *Neurology,* in press.
24. Daggett, V. & Levitt, M. (1993). Realistic simulations of native-protein dynamics in solution and beyond. *Annu. Rev. Biophy. Biomol. Struct.* **22**, 353–380.
25. Brooks, C. & Case, D. (1993). Simulations of peptide conformational dynamics and thermodynamics. *Chem. Rev.* **93**, 2487–2502.
26. Levitt, M. & Perutz, M.F. (1988). Aromatic rings act as hydrogen bond acceptors. *J. Mol. Biol.* **201**, 751–754.
27. Burley, S.K. & Petsko, G.A. (1986). Amino–aromatic interactions in proteins. *FEBS Lett.* **203**, 139–143.
28. Borchelt, D.R., Scott, M., Taraboulos, A., Stahl, N. & Prusiner, S.B. (1990). Scrapie and cellular prion proteins differ in their kinetics of synthesis and topology in cultured cells. *J. Cell Biol.* **110**, 743–752.
29. Borchelt, D.R., Taraboulos, A. & Prusiner, S.B. (1992). Evidence for synthesis of scrapie prion proteins in the endocytic pathway. *J. Biol. Chem.* **267**, 16188–16199.

30. Nguyen, J., Baldwin, M.A., Cohen, F.E. & Prusiner, S.B. (1995). Prion protein peptides induce α-helix to β-sheet conformational transitions. *Biochemistry* **34**, 4186–4192.
31. Padmanabhan, S., Marqusee, S., Ridgeway, T., Laue, T.M., & Baldwin, R.L. (1990). Relative helix-forming tendencies of nonpolar amino acids. *Nature* **344**, 268–270.
32. Padmanabhan, S. & Baldwin, R.L. (1991). Straight-chain non-polar amino acids are good helix formers in water. *J. Mol. Biol.* **219**, 135–137.
33. Levitt, M. (1990). ENCAD—Energy Calculations and Dynamics. Molecular Applications Group. Stanford University, Palo Alto, CA.
34. Levitt, M. (1983). Molecular dynamics of native protein. I. Computer simulation of trajectories. *J. Mol. Biol.* **168**, 595–620.
35. Levitt, M. (1989). Molecular dynamics of macromolecules in water. *Chemica Scripta* **29A**, 197–203.
36. Levitt, M., Hirshberg, M., Sharon, R., & Daggett, V. (1995). Potential energy function and parameters for simulations of the molecular dynamics of proteins and nucleic acids in solution. *Comp. Phys. Commun.*, in press.
37. Daggett, V. & Levitt, M. (1992). Molecular dynamics simulations of helix denaturation. *J. Mol. Biol.* **223**, 1121–1138.
38. Daggett, V., Kollman, P.A. & Kuntz, I.D. (1991). A molecular dynamics simulation of polyalanine: an analysis of equilibrium motions and helix-coil transitions. *Biopolymers* **31**, 1115–1134.
39. Ferrin, T.E., Huang, L.E., Jarvis, L.E. & Langridge, R. (1988). The MIDAS display system. *J. Mol. Graph.* **6**, 13–27.

Received: **6 Mar 1995**; revisions requested: **27 Mar 1995**; revisions received: **20 Apr 1995**. Accepted **1 May 1995**.